

Experimental Multi-Qubit Robustness by Local Encoding

Massimiliano Proietti,¹ Martin Ringbauer,^{1,2} Francesco Graffitti,¹ Peter Barrow,¹ Alexander Pickston,¹ Dmytro Kundys,¹ Daniel Cavalcanti,³ Leandro Aolita,⁴ Rafael Chaves,^{5,6} and Alessandro Fedrizzi¹

¹*Scottish Universities Physics Alliance (SUPA), Institute of Photonics and Quantum Sciences, School of Engineering and Physical Sciences, Heriot-Watt University, Edinburgh EH14 4AS, UK*

²*Institut für Experimentalphysik, Universität Innsbruck, 6020 Innsbruck, Austria*

³*ICFO-Institut de Ciències Fotoniques, The Barcelona Institute of Science and Technology, 08860 Castelldefels (Barcelona), Spain*

⁴*Instituto de Física, Universidade Federal do Rio de Janeiro, P. O. Box 68528, Rio de Janeiro, RJ 21941-972, Brazil*

⁵*International Institute of Physics, Federal University of Rio Grande do Norte, 59070-405 Natal, Brazil*

⁶*School of Science and Technology, Federal University of Rio Grande do Norte, 59078-970 Natal, Brazil*

The first generation of many-body quantum technologies will consist of noisy, intermediate-scale devices for which active error correction remains out of reach. To exploit such devices, it is imperative to use passive error protection that meets a careful trade-off between noise protection and resource overhead. Here, we experimentally demonstrate that single-qubit encoding can significantly enhance the robustness of entanglement and coherence of four-qubit graph states against local noise with a preferred axis. In particular, we show that, in some cases, finite-time disentanglement is asymptotically turned into non-zero entanglement. Finally, we explicitly show that local encoding provides a significant practical advantage for phase estimation in noisy environments. This demonstrates the efficacy of local unitary encoding under realistic conditions, with potential applications in multi-qubit quantum technologies for metrology, multi-partite secrecy and error correction.

INTRODUCTION

Quantum systems are notoriously fragile due to unavoidable interactions with their environment [1], resulting in decoherence that grows exponentially with system size. This represents a major roadblock for quantum computing [2], quantum communication [3] and quantum metrology [4], rendering noise mitigation [5–7] indispensable. Quantum error correction (QEC) [8–10] schemes in principle achieve full protection against decoherence. However, daunting experimental requirements on the single qubit noise rate and large resource overheads [11] make full QEC a long-term vision.

A complementary approach, which is expected to play a central role in near-term quantum technologies [12], is to relax the requirement of fault-tolerance against arbitrary noise and instead aim at increasing the robustness of quantum systems under specific, experimentally relevant conditions. One of the dominant types of noise in most experiments is local dephasing [2] along a privileged direction [13–15]. There, simple single-qubit unitary encoding can drastically improve the resilience of quantum resources [16] such as the paradigmatic multi-qubit Greenberger-Horne-Zeilinger (GHZ) [17] states, where an exponential decay of entanglement [18, 19] can be turned into a linear decay [16]. This improvement is crucial for metrology applications such as phase estimation in noisy environments [20, 21], whereby the otherwise optimal GHZ states [22] quickly lose their advantage under dephasing and become asymptotically bounded in phase sensitivity by a constant [23].

Here, in a state-of-the-art 4-photon experiment, we re-

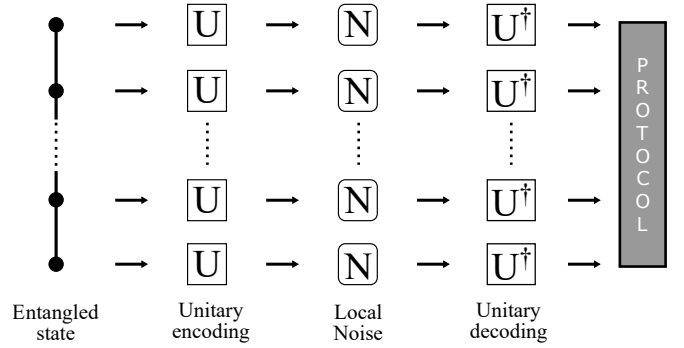


FIG. 1. Enhanced noise robustness with local encoding. An N -qubit entangled state is subject to local dephasing along the z -direction, before it is used for a task such as quantum phase estimation. We use a single-qubit unitary encoding before and after the noise to optimally protect the state’s entanglement and coherence, so as to improve its performance in the final metrology task.

port an in-depth study of the enhanced resilience that can be gained from local encoding [16] under realistic conditions, see Fig. 1. Using symmetric informationally complete (SIC) [24] tomographic techniques, we experimentally quantify the noise resilience of quantum resources such as coherence and entanglement for all local-unitarily inequivalent classes of 4-qubit graph states [25, 26]. Contrary to intuition, we sometimes find that single-qubit encoding achieving optimal noise protection, are also found to generate more entanglement with the environment (therefore decreasing the state’s purity).

Finally, as quantified by the experimental phase variance and the quantum Fisher information [27], we observe that our encoding provides a clear improvement

of the usefulness of 4-qubit GHZ states for noisy quantum phase estimation. Notably, even under full dephasing, where the entanglement is always zero, the states nonetheless remain useful. This suggests a key role played by coherence, which instead is shown to be independent from the noise when the encoding is applied.

In the following, we first describe the theoretical background the experiment is based on. We then present in detail the experimental setup, followed by the results showing the effects of the local-encoding on purity, entanglement and coherence. Finally, after reviewing the basic concepts of phase estimation, we conclude proving the immediate advantage of our experimentally-friendly encoding in noisy phase estimation.

BACKGROUND

Consider an ideal quantum system being subject to local dephasing noise for a finite period of time, before being used for a information-processing task. Our aim is to encode the system before the noise acts in order to increase its resilience against dephasing with as simple an encoding as possible, and then decode the system before it is being used, see Fig. 1. Taking the dephasing to act on the state ρ in the computational basis $\{|0\rangle, |1\rangle\}$, the single-qubit dephasing channel is given by

$$\mathcal{D}(\rho) \doteq \left(1 - \frac{p}{2}\right) \rho + \frac{p}{2} \sigma_z \rho \sigma_z, \quad (1)$$

where $\sigma_z = |0\rangle\langle 0| - |1\rangle\langle 1|$ is the Z Pauli matrix, and $0 \leq p \leq 1$ determines the noise strength from no noise ($p = 0$) to full dephasing ($p = 1$). Consider now, for instance, an N -qubit GHZ state defined as

$$|GHZ_N\rangle \doteq \frac{1}{\sqrt{2}} (|0\rangle^{\otimes N} + |1\rangle^{\otimes N}) \quad (2)$$

The entanglement of GHZ states under single-qubit dephasing is known to decay exponentially with N . More precisely, for the dephased GHZ state $\rho_N(p) \doteq \mathcal{D}^{\otimes N}(|GHZ_N\rangle\langle GHZ_N|)$ it holds that $E(\rho_N(p)) \leq (1-p)^N E(\rho_N(0))$ for any convex entanglement quantifier E [18, 19]. However, this scaling can be drastically improved [16] by encoding the state using local Hadamard gates H , defined by $H|0\rangle \doteq |+\rangle$ and $H|1\rangle \doteq |-\rangle$ with $|\pm\rangle \doteq \frac{1}{\sqrt{2}}(|0\rangle \pm |1\rangle)$. The resulting *transversally encoded* GHZ state:

$$|GHZ_N^{enc}\rangle \doteq H^{\otimes N} |GHZ_N\rangle = \frac{1}{\sqrt{2}} (|+\rangle^{\otimes N} + |-\rangle^{\otimes N}) \quad (3)$$

has the same entanglement properties, yet its entanglement decay rate becomes independent of N and linear in p . Formally, the dephased encoded state $\rho_N^{enc}(p) \doteq \mathcal{D}^{\otimes N}(|GHZ_N^{enc}\rangle\langle GHZ_N^{enc}|)$ satisfies the bound $E(\rho_N^{enc}(p)) \geq E(\rho_2(p))$ for all N and thus possesses at

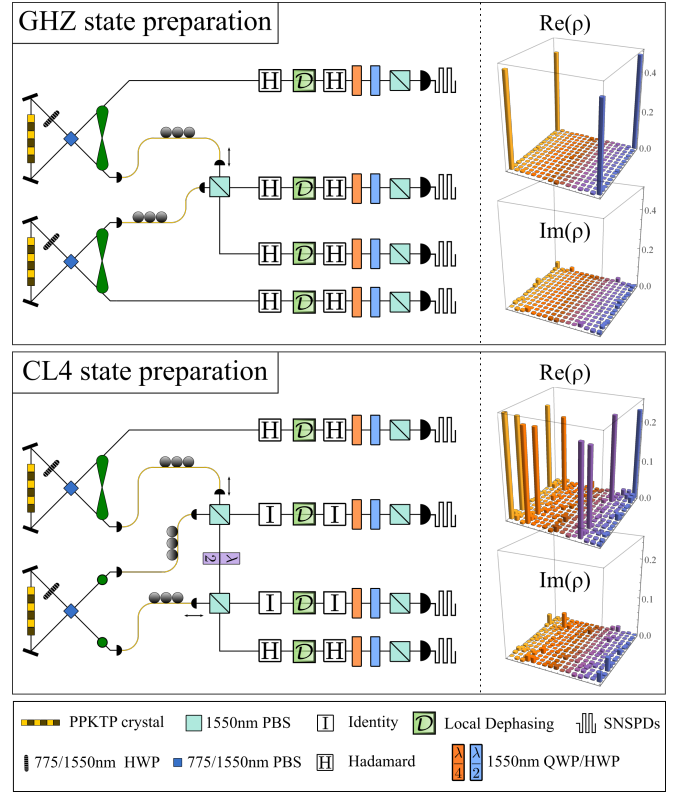


FIG. 2. **Preparation of 4-qubit GHZ (top) and linear cluster (bottom) states and encoding stage.** Pairs of photons at 1550 nm are generated via spontaneous parametric downconversion in periodically-poled KTP (PPKTP) crystals. The GHZ state is obtained from interfering photons from two entangled pairs on a polarizing beam splitter (PBS), while the linear cluster is obtained from two successive interference of one photon from an entangled pair with two diagonally polarized single photons. The encoding in both cases corresponds to single-qubit Hadamard (H) gates or identity (I) operations. The state is then locally encoded, dephased, decoded, and measured using a combination of quarter-waveplate (QWP), half-waveplate (HWP), PBS, and superconducting nanowire single photon detectors (SNSPDs) with four-fold coincidence detection. On the right, the real and imaginary part of the experimental density matrices (without dephasing) are shown. For the GHZ is the bare state whereas for the linear cluster is the encoded state.

least as much resilience as the two-qubit state $|GHZ_2\rangle$. A similar enhancement can be achieved for arbitrary graph states, which play a crucial role in measurement-based quantum computing and quantum error correction.

For $N = 4$ qubits there exist only two equivalence classes of connected graph states under local unitary transformation [26]. The paradigmatic representatives of these two families are the GHZ state $|GHZ_4\rangle$ and the linear cluster state $|CL_4\rangle$, with the latter commonly de-

fined as

$$\begin{aligned} |CL_4\rangle &\doteq CZ_{1,2}CZ_{2,3}CZ_{3,4}HHHH|0000\rangle = \\ &= \frac{1}{2}(|+00+\rangle + |-10+\rangle + \\ &\quad + |+01-\rangle - |-11-\rangle), \end{aligned} \quad (4)$$

where the tensor product is omitted and $CZ_{i,j}$ is a controlled-Z gate [2] on qubits i and j . This expression corresponds to the graph state represented as a linear chain with qubits 1, 4 as external vertices. The optimal local-unitary encoding for protecting the entanglement of $|CL_4\rangle$ turns out to be $H \otimes \mathbb{1} \otimes \mathbb{1} \otimes H$, with $\mathbb{1}$ the single-qubit identity operator, resulting in the state

$$|CL_4^{enc}\rangle = \frac{1}{2}(|0000\rangle + |1100\rangle + |0011\rangle - |1111\rangle) \quad (5)$$

By investigating both the GHZ and the linear cluster quantum states, our experiment thus in essence covers all 4-qubit graph states.

EXPERIMENTAL SETUP

We now test these passive error protection techniques in a state-of-the-art photonic platform, Fig. 2. Qubits are encoded in the horizontal $|h\rangle = |0\rangle$ and vertical $|v\rangle = |1\rangle$ polarization states of single photons. These are generated at 1550 nm via collinear type-II spontaneous parametric down-conversion in a 22 mm long periodically-poled KTP (PPKTP) crystal, pumped with a 1.6 ps pulsed laser at 775 nm [28]. After spectral filtering with a bandwidth of 3 nm, the source generates ~ 3075 pairs/mW/s with a symmetric heralding efficiency of $\sim 55\%$. Embedding the crystal within a Sagnac interferometer [29] enables the generation of high-quality entangled states of the form

$$|\psi^-\rangle = \frac{1}{\sqrt{2}}(|h\rangle|v\rangle - |v\rangle|h\rangle), \quad (6)$$

with typical fidelities of $\mathcal{F} = 99.62^{+0.01}_{-0.04}\%$, purity $\mathcal{P} = 99.34^{+0.01}_{-0.09}\%$ and entanglement as measured by the concurrence [30] $\mathcal{C} = 99.38^{+0.02}_{-0.10}\%$. The photons are detected using superconducting nano-wire single-photon detectors (SNSPDs) with an efficiency of $\sim 80\%$ and processed using a time-tagging module with a resolution of 156 ps.

Using two such photon-pair sources in the setup of Fig. 2, we generate the representative states of the two inequivalent classes of 4-qubit graph states: the GHZ state $|GHZ_4\rangle$ of Eq. (2), and the linear cluster of Eq (5) at a measured rate of 47.6 Hz using 60 mW pump power. The GHZ state $|GHZ_4\rangle$ is prepared by subjecting one photon of each entangled pair to nonclassical interference on a polarizing beam splitter (PBS), which transmits horizontal and reflects vertically polarized photons. This implements a so-called type-I fusion gate [31] for

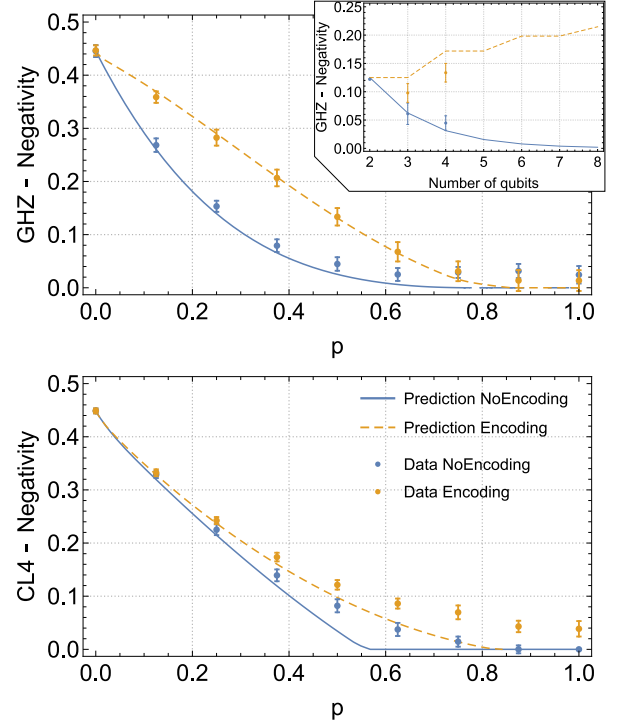


FIG. 3. **Resilience enhancement of the negativity [32] in the partition (1|234).** Shown is the negativity of the GHZ (top) and linear cluster (bottom) with (dashed-orange) and without (solid-blue) encoding. The solid (dashed) lines depict the theoretical predictions with the experimental bare (encoded) input state. In the top-right inset the trend of the GHZ negativity is shown in terms of the number of qubits and at fixed noise $p = 0.5$. With the encoding proposed, the entanglement is best protected when the number of qubits increases. Error bars represent 3σ statistical confidence regions obtained from a Monte-Carlo routine taking into account the Poissonian counting statistics.

which we achieved a visibility of $91.80^{+1.73}_{-1.73}\%$, translating into a purity of $\mathcal{P} = 87.09^{+1.15}_{-2.18}\%$ and fidelity of $\mathcal{F} = 92.53^{+0.63}_{-1.23}\%$ for the 4-qubit GHZ state. The linear cluster $|CL_4^{enc}\rangle$, on the other hand, is generated by subjecting one photon of an entangled pair to two sequential fusion gates with uncorrelated single photons in the state $|+\rangle$ and with a Hadamard gate in between. This results in slightly lower purity of $\mathcal{P} = 81.77^{+0.65}_{-0.85}\%$ and fidelity of $\mathcal{F} = 89.03^{+0.38}_{-0.60}\%$.

Single qubit dephasing of Eq. (1) is experimentally implemented in a controllable manner by applying individual phase flips, using HWPs, to a fraction of the experimental runs weighted by the dephasing strength p . The density matrices of the experimentally generated states are then reconstructed using maximum-likelihood quantum state tomography. The tomography was performed using the set of symmetric informationally complete (SIC) measurements [24], which reduces the number of measurements compared to the standard Pauli basis by a factor $(2/3)^N$, leading to improved precision at equal

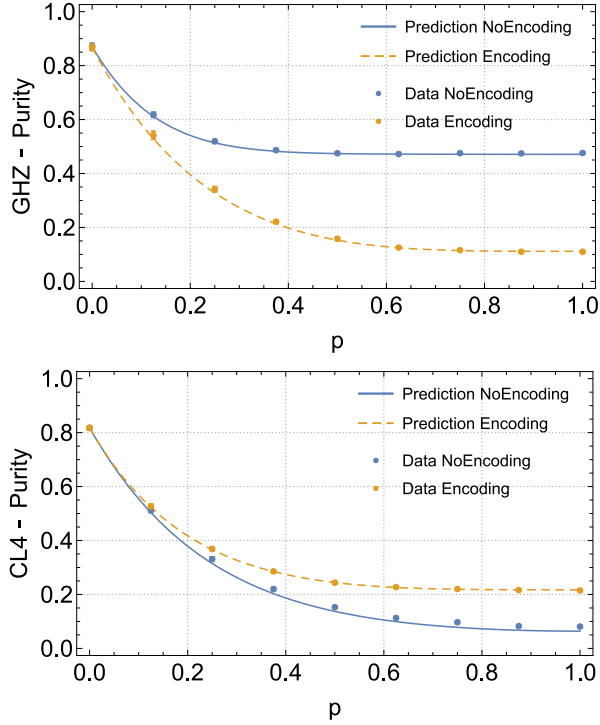


FIG. 4. **Experimental results for the purity under local encoding.** Shown is the purity of the GHZ (top) and linear cluster (bottom) states with (dashed-orange) and without (solid-blue) encoding. The solid (dashed) lines depict the theoretical predictions with the experimental bare (encoded) input state. Interestingly, conversely to the GHZ case, the purity of the linear cluster is enhanced by the local encoding. The 3σ error bars, obtained as previously, are smaller than the symbol size.

acquisition time.

EXPERIMENTAL NOISE PROTECTION

In this section we present the experimental results at-testing the capability of the method proposed. We start by investigating one of the most paradigmatic quantum resources: quantum entanglement, as measured by the negativity in the partition $(1 | 234)$. Other partitions give qualitatively similar results, although typically require different encoding, see SM for details. Figure 3 shows that the negativity of the encoded $|GHZ_4^{enc}\rangle$ and $|CL_4^{enc}\rangle$ states is significantly more resilient against dephasing than the bare states. In the case of the linear cluster, it is even possible to qualitatively change the behavior from finite-time disentanglement to infinite-time disentanglement. Moreover, the inset in Fig. 3 confirms in the case of GHZ states (note that for $N < 4$ the linear cluster and the GHZ are equivalent), that the enhancement for a fixed amount of dephasing becomes more significant as the number of qubits increases, instead of the

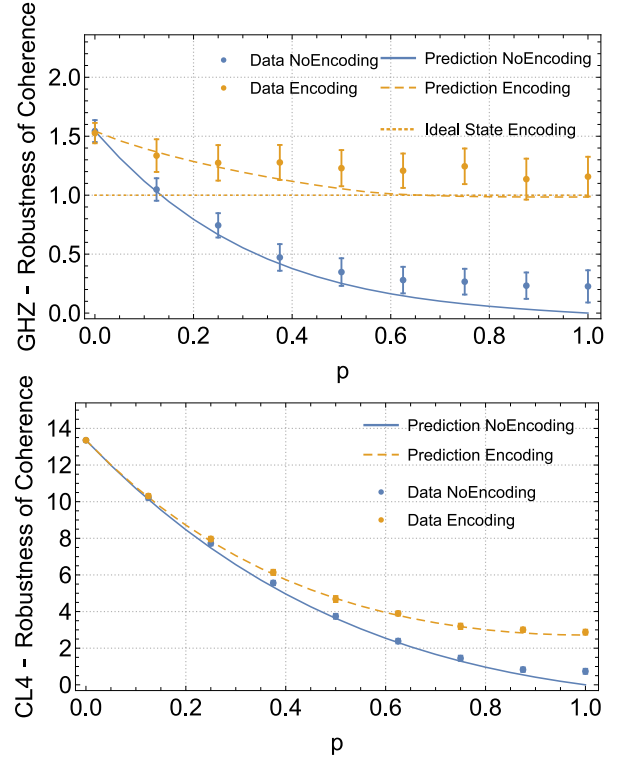


FIG. 5. **Resilience of coherence against dephasing noise.** Robustness of coherence R_{C_1} for the 4-qubit GHZ (top) and linear cluster state (bottom). The solid-blue lines represent the theory prediction when the states are not encoded, compared with the encoded scenario given by the dashed-orange lines. For the GHZ state only, the theory prediction starting with an ideal input encoded state is shown with a dotted-orange curve. Note that experimental imperfections tend to lead to additional coherence terms compared to the ideal GHZ state. The robustness of coherence reflects this as higher initial values of coherence and non-vanishing coherence for all dephasing strengths. Experimental data is shown as blue (orange) dots for the non-encoded (encoded) case with 3σ error bars smaller than the symbol size

exponential decay observed for the bare states [16]. Intuitively, one would assume that the noise resilience is achieved by reducing the amount of entanglement with the environment that is generated (thus increasing the state's purity). Surprisingly, however, the results of Fig. 4 show that, for the GHZ case, the opposite is true and the encoded states experience a higher loss of purity than the non-encoded ones. This can be understood as a consequence of the special structure of the GHZ state, which even after full dephasing retains classical correlations that manifest in relatively high residual purity. In the encoded case, the coherence is more distributed, thereby reducing the resilience of the state's purity. In the case of the linear cluster, on the other hand, the bare state features uniformly distributed populations, while the encoded state is sparser. As a consequence, the optimal encoding protects both entanglement *and* purity.

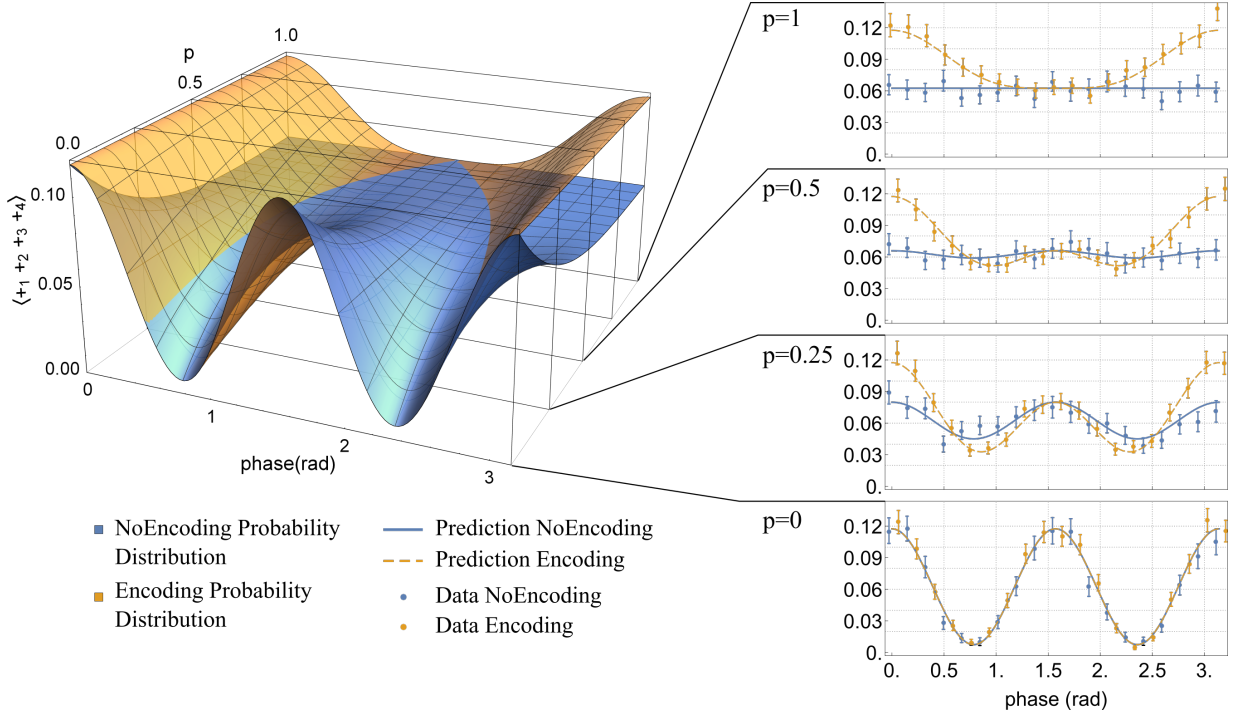


FIG. 6. **Phase estimation with and without encoding.** **Left** Expectation value $\langle +_1 +_2 +_3 +_4 \rangle$ as a function of phase and amount of noise p , for a locally encoded (orange) and a non-encoded (blue) 4-qubit GHZ state. **Right** Experimentally measured expectation values $\langle +_1 +_2 +_3 +_4 \rangle$ as a function of the phase for varying dephasing strength. The theoretical predictions are shown as blue-solid (no encoding) and orange-dashed (encoding) curves, and error bars indicate 3σ statistical uncertainty regions obtained from a Monte Carlo resampling of our Poisson counting statistics. In the absence of noise ($p = 0$) there is no difference between encoded and bare states. With increasing dephasing, however, the advantage of the encoding becomes clear in that the expectation values for bare states decay to zero, but remain non-zero for all p if the local encoding is used.

State	Encoding	Entanglement	Purity	Coherence
$ GHZ_4\rangle$	HHHH	✓	X	✓
$ CL_4\rangle$	H11H	✓	✓	✓

TABLE I. Comparison of the encoding effect for GHZ and linear cluster states. The ✓ symbol corresponds to enhancement of the encoded state respect to the non encoded one, for the respective quantity labeled in each column.

The final piece in the puzzle is thus the behavior and structure of the states' coherence under dephasing. Using the recently developed resource theory of multilevel coherence [33, 34] we can quantify the decay of coherence under dephasing noise, see SM for details. Multi-level coherence is independent of entanglement measures, therefore unlocks information on the encoding effects otherwise inaccessible. This, as we will see in the next section, provides useful insights on phase estimation in noisy environment. Intriguingly, the top panel in Fig. 5 shows that our encoded GHZ_4 states maintain a constant amount of coherence for arbitrary dephasing, while the bare states show an exponential decay. Intuitively, this may again be understood based on the distribution of coherence within

the state. Concentrating all coherence on two terms (coherence rank 2), such as the bare GHZ_4 state leaves the state vulnerable to dephasing, as opposed to maximally spreading it out (coherence rank 2^N), such as the encoded state, achieving increased resilience. In the latter case indeed, the decoding map (a non-free operation in the resource theory of coherence) can under certain conditions recover a significant amount of coherence, see SM for details.

On the other hand, for the linear cluster in the bottom panel of Fig. 5, constant behavior cannot be achieved, due to subtle differences in the structure of the states. Nonetheless protection is observed for all the values of dephasing. This behavior is confirmed at all coherence levels, see SM.

The results just presented, for entanglement purity and negativity are summarized in Table I.

ENHANCED PHASE ESTIMATION

We now exploit our passive error correction for quantum metrology, by performing a 4-qubit phase estimation task [35] in a noisy environment. The goal is to estimate an unknown phase ϕ imparted on a probe state

p	No enc $Var[\phi](10^{-5})$	Enc $Var[\phi](10^{-5})$
0	10.67	8.99
0.125	42.20	17.91
0.25	151.90	30.03
0.5	5095.68	66.41
0.75	43822	144.93
1	∞	191.72

TABLE II. Comparison of the phase variance without (2nd column) and with (3rd column) encoding, for different noise strengths. The values shown are in the order of 10^{-5} radian. Notably, with encoding, the variance observed is up to 2 orders of magnitude smaller than the case without, where the error on the inferred phase diverges with increasing noise.

ρ by the unitary $U_\phi = e^{-\frac{i}{2}\phi\sigma_z}$ by appropriately measuring the evolved state $\rho_\phi \doteq U_\phi^{\otimes N} \rho U_\phi^{\dagger \otimes N}$. It is well known that GHZ states with local measurements in the Pauli-X basis are optimal for phase estimation [4]. In the presence of dephasing noise, however, this task becomes much more challenging, and different inequivalent strategies can be devised [36]. We now show how our local encoding can significantly enhance the metrology performance of 4-qubit GHZ state under such conditions. To assess the performance of phase estimation we study the expectation value:

$$\text{Tr}[\rho_\phi (|+\rangle\langle+|)^{\otimes 4}]_{\text{GHZ}} = \frac{1}{16} ((p-1)^4 \cos(4\phi) + 1),$$

for noise of strength p , showing that for maximal dephasing, $p \rightarrow 1$, no phase information can be recovered. Conversely, if the local encoding of Eq. (3) is used, we find improved performance for all p . Most strikingly, the encoding preserves phase sensitivity even under full dephasing ($p = 1$):

$$\text{Tr}[\rho_\phi (|+\rangle\langle+|)^{\otimes 4}]_{\text{GHZ}^{\text{enc}}} = \frac{1}{128} (4 \cos(2\phi) + \cos(4\phi) + 11).$$

Is important to note that in the full dephasing regime, the entanglement as measured by the negativity is always zero, even for the encoded states. It follows that the phase sensitivity observed is instead provided by the coherence only, which as we have previously seen is left untouched by the dephasing. Only when both coherence and entanglement are zero (as for the non-encoded states) the phase sensitivity is completely suppressed. This suggests the coherence to be a useful resource whereby the entanglement is not.

Experimentally, we applied a phase-shift $\phi \in [0, \pi]$ to each qubit, by shifting the measurement's waveplates accordingly and reconstructed the expectation values $\text{Tr}[\rho_\phi (|+\rangle\langle+|)^{\otimes 4}]$ for a range of p , see Fig. 6. These results clearly show a steeper slope of $\text{Tr}[\rho_\phi (|+\rangle\langle+|)^{\otimes 4}]$ as a function of ϕ for the encoded state compared to the bare state for all non-zero values of ϕ . This directly translates into a more sensitive phase estimator in the encoded

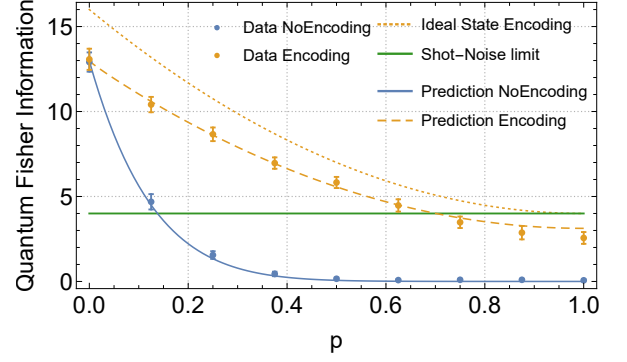


FIG. 7. **Robustness enhancement of the quantum Fisher information.** QFI of the encoded (dashed-orange) and non-encoded (solid-blue) states, compared with the shot-noise limit (solid green). Experimental data are shown with error bars equivalent to 3σ statistical confidence regions. Without encoding, the GHZ state loses its advantage already in the low-noise regime. In contrast, as shown in the figure, the encoding preserves the QFI for all values of dephasing, ideally (dotted-orange), and up to $p=0.6$ experimentally.

case. Moreover, we emphasize that the encoded fringes preserve at least half the visibility of the $p = 0$ case, even in the case of full dephasing where instead, without our experimentally friendly encoding, the bare fringes flatten to a constant value. In other words, where phase estimation would be normally impossible, our encoding makes it feasible again.

This qualitative behavior is turned into a quantitative result by measuring the experimental variance of the estimated phase in the point where the fringes are the steepest for different values of p , see II. The variance of the phase is computed by propagating the error on the estimator according to

$$Var[\phi] = \frac{Var[\epsilon]}{|\frac{d}{d\phi}\epsilon|^2}, \quad (7)$$

where ϵ is the measured average value of our estimator $\epsilon \equiv \langle +_1 +_2 +_3 +_4 \rangle$.

More in general however, the primary figure of merit in quantum metrology is the so called *quantum Fisher information* (QFI) [27]. Indeed, in the noiseless case, the statistical deviation $\delta\phi$ in the estimation of ϕ , is bounded as $\delta\phi \geq 1/\left(\sqrt{\nu\mathcal{F}(\rho_\phi)}\right)$ [37], where ν is the number of repetition runs in the estimation and $\mathcal{F}(\rho_\phi)$ is the QFI, measuring the maximum amount of information about ϕ that can be extracted from ρ_ϕ . For separable states $\mathcal{F}(\rho_\phi) \leq N$, namely the QFI is bounded by the shot-noise limit (SNL), while for GHZ states the QFI attains the optimal value $\mathcal{F}_{\text{max}} = N^2$, known as the Heisenberg limit. On the other hand, the QFI of a locally dephased GHZ state $\mathcal{F}(\rho_N(p)) = N^2(1-p)^{2N}$, indicates that for fixed noise strength p the precision of the estimate of ϕ decreases

exponentially with N . The transversally encoded GHZ state, however, does not show this dramatic drop and instead exhibits $\mathcal{F}(\rho_N^T(p)) = N^2(1-p)^2 + 4N(1-\frac{p}{2})\frac{p}{2}$. Consequently, the local encoding also boosts the accuracy in phase estimation from an exponential decay with N to a quadratic one. We numerically compute the eigenvalues and eigenvectors of the experimental matrices, see SM Fig. S2 and, using the formalism in [38] with Hamiltonian $H = \frac{1}{2} \sum_i Z_i$, we compute the value of the quantum Fisher information, shown in Fig. 7. In absence of noise we experimentally observe a value close to the Heisenberg limit $N^2 = 16$ for bare GHZ states. However, already for relatively low noise strengths, we find the QFI of bare states (solid-blue in the figure) drops below the SNL. Remarkably, transversally-encoded GHZ states (dashed-orange) preserve their quantum advantage for significantly higher noise strengths, as shown in Fig. 7. Notably, with ideal initial states the QFI is expected to reach the SNL only asymptotically for full dephasing $p = 1$. However, even under imperfect experimental conditions, we maintain above-SNL performance into the high-noise regime of up to $p = 0.6$.

CONCLUSIONS

Active multi-qubit quantum error correction remains out of reach for current technology. Even once it becomes feasible, the overheads it involves imply that passive noise protection will still play a central role in quantum technologies. We have shown that, given knowledge of the dominant noise sources in the experiment, protection of quantum resources without complex encoding and additional overhead in the number of physical qubits, is feasible in practice and can enable significant performance improvements. Since this approach relies on the structure of the quantum states under investigation, protecting different quantum resources typically requires different encoding. We revealed different behaviors of graph states for all the quantum figure of merits under study, highlighting the importance of a deep understanding of state dynamics in the multi-qubit scenario. Applying the suggested encoding in a noisy phase estimation protocol, we furthermore unveiled a scenario where only coherence and not entanglement is the useful resource for such task. In conclusion, the passive encoding demonstrated here succeeds at protecting the most important quantum features of crucial many-qubit states with no overhead whatsoever in ancillary qubits; and could furthermore be combined with active error correction primitives. We expect it to be a useful tool for large-scale quantum information devices in realistic, noisy conditions.

This work was supported by the UK Engineering and Physical Sciences Research Council (grant number EP/N002962/1), the Ramón y Cajal fellowship (Spain), Spanish MINECO (QIBEQI FIS2016-80773-P

and Severo Ochoa SEV-2015-0522), the AXA Chair in Quantum Information Science, Generalitat de Catalunya (SGR875 and CERCA Programme), Fundació Privada Cellex and ERC CoG QITBOX. FG acknowledges studentship funding from EPSRC under grant no. EP/L015110/1. LA acknowledges financial support from the Brazilian agencies CNPq (PQ grant No. 311416/2015-2 and INCT-IQ), FAPERJ (JCN E-26/202.701/2018), CAPES (PROCAD2013), FAPESP, and the Serrapilheira Institute (grant number Serra-1709-17173). RC acknowledges the Brazilian ministries MEC and MCTIC, funding agency CNPq (PQ grants No. 307172/2017-1 and No 406574/2018-9 and INCT-IQ), the John Templeton Foundation via the grant Q-CAUSAL No. 61084 and the Serrapilheira Institute (grant number Serra-1708-15763).

-
- [1] W. H. Zurek, Decoherence, einselection, and the quantum origins of the classical, *Rev. Mod. Phys.* **75**, 715 (2003).
 - [2] M. A. Nielsen and I. L. Chuang, *Quantum Computation and Quantum Information: 10th Anniversary Edition*, 10th ed. (Cambridge University Press, 2011).
 - [3] H. Aschauer and H. J. Briegel, *Coherent Evolution in Noisy Environments*, edited by A. Buchleitner and K. Hornberger (Springer Berlin Heidelberg, Berlin, Heidelberg, 2002) pp. 235–261.
 - [4] V. Giovannetti, S. Lloyd, and L. Maccone, Advances in quantum metrology, *Nat. Photon.* **5**, 222 (2011).
 - [5] M. Freedman, A. Kitaev, M. Larsen, and Z. Wang, Topological quantum computation, *Bulletin Am. Math. Soc.* **40**, 31 (2003).
 - [6] D. A. Lidar, I. L. Chuang, and K. B. Whaley, Decoherence-free subspaces for quantum computation, *Phys. Rev. Lett.* **81**, 2594 (1998).
 - [7] Y. S. Kim, J. C. Lee, O. Kwon, and Y. H. Kim, Protecting entanglement from decoherence using weak measurement and quantum measurement reversal, *Nat. Phys.* **8**, 117 (2012).
 - [8] P. W. Shor, Scheme for reducing decoherence in quantum computer memory, *Phys. Rev. A* **52**, 2493 (1995).
 - [9] A. R. Calderbank and P. W. Shor, Good quantum error-correcting codes exist, *Phys. Rev. A* **54**, 1098 (1996).
 - [10] A. M. Steane, Error Correcting Codes in Quantum Theory, *Phys. Rev. Lett.* **77**, 793 (1996).
 - [11] D. Aharonov and M. Ben-Or, Fault-Tolerant Quantum Computation with Constant Error Rate, *SIAM J. Comp.* **38**, 1207 (2008).
 - [12] J. Preskill, Quantum Computing in the NISQ era and beyond, *Quantum* **2**, 79 (2018).
 - [13] J. Noda, K. Okamoto, and Y. Sasaki, Polarization-maintaining fibers and their applications, *J. of Lightwave Tech.* **4**, 1071 (1986).
 - [14] D. Leibfried, R. Blatt, C. Monroe, and D. Wineland, Quantum dynamics of single trapped ions, *Rev. Mod. Phys.* **75**, 281 (2003).
 - [15] P. Schindler, D. Nigg, T. Monz, J. T. Barreiro, E. Martinez, S. X. Wang, S. Quint, M. F. Brandl, V. Nebendahl,

- C. F. Roos, M. Chwalla, M. Hennrich, and R. Blatt, A quantum information processor with trapped ions, *New J. Phys.* **15**, 123012 (2013).
- [16] R. Chaves, L. Aolita, and A. Acín, Robust multipartite quantum correlations without complex encodings, *Phys. Rev. A* **86**, 020301 (2012).
- [17] D. M. Greenberger, M. A. Horne, A. Shimony, and A. Zeilinger, Bell's theorem without inequalities, *Am. J. Phys.* **58**, 1131 (1990).
- [18] L. Aolita, R. Chaves, D. Cavalcanti, A. Acín, and L. Davidovich, Scaling laws for the decay of multiqubit entanglement, *Phys. Rev. Lett.* **100**, 080501 (2008).
- [19] L. Aolita, F. de Melo, and L. Davidovich, Open-system dynamics of entanglement: a key issues review, *Rep. Prog. Phys.* **78**, 042001 (2015).
- [20] A. Shaji and C. M. Caves, Qubit metrology and decoherence, *Phys. Rev. A* **76**, 032111 (2007).
- [21] R. Chaves, J. B. Brask, M. Markiewicz, J. Kołodyński, and A. Acín, Noisy metrology beyond the standard quantum limit, *Phys. Rev. Lett.* **111**, 120401 (2013).
- [22] V. Giovannetti, S. Lloyd, and L. Maccone, Quantum-enhanced measurements: beating the standard quantum limit, *Science* **306**, 1330 (2004).
- [23] R. Demkowicz-Dobrzański, J. Kołodyński, and M. Guţă, The elusive heisenberg limit in quantum-enhanced metrology, *Nat. Commun.* **3**, 1063 (2012).
- [24] J. M. Renes, R. Blume-Kohout, A. J. Scott, and C. M. Caves, Symmetric informationally complete quantum measurements, *J. Math. Phys.* **45**, 2171 (2004).
- [25] M. HEIN, Entanglement in graph states and its applications, Proc. International School of Physics " Enrico Fermi " on " Quantum Computers, Algorithms and Chaos," Varenna, Italy, July 2005 (2005).
- [26] M. Hein, J. Eisert, and H. J. Briegel, Multiparty entanglement in graph states, *Phys. Rev. A* **69**, 062311 (2004).
- [27] A. S. Holevo, *Probabilistic and statistical aspects of quantum theory*, Vol. 1 (Springer Science & Business Media, 2011).
- [28] F. Graffitti, J. Kelly-Massicotte, A. Fedrizzi, and A. M. Brańczyk, Design considerations for high-purity heralded single-photon sources, *Phys. Rev. A* **98**, 053811 (2018).
- [29] A. Fedrizzi, T. Herbst, A. Poppe, T. Jennewein, and A. Zeilinger, A wavelength-tunable fiber-coupled source of narrowband entangled photons, *Opt. Express* **15**, 15377 (2007).
- [30] S. Hill and W. K. Wootters, Entanglement of a Pair of Quantum Bits, *Phys. Rev. Lett.* **78**, 5022 (1997).
- [31] D. E. Browne and T. Rudolph, Resource-Efficient Linear Optical Quantum Computation, *Phys. Rev. Lett.* **95**, 010501 (2005).
- [32] G. Vidal and R. F. Werner, Computable measure of entanglement, *Phys. Rev. A* **65**, 032314 (2002).
- [33] C. Napoli, T. R. Bromley, M. Cianciaruso, M. Piani, N. Johnston, and G. Adesso, Robustness of Coherence: An Operational and Observable Measure of Quantum Coherence, *Phys. Rev. Lett.* **116**, 150502 (2016).
- [34] M. Ringbauer, T. R. Bromley, M. Cianciaruso, L. Lami, W. Y. S. Lau, G. Adesso, A. G. White, A. Fedrizzi, and M. Piani, Certification and quantification of multilevel quantum coherence, *Phys. Rev. X* **8**, 041007 (2018).
- [35] G. Tóth and I. Apellaniz, Quantum metrology from a quantum information science perspective, *J. Phys. A* **47**, 424006 (2014).
- [36] R. Demkowicz-Dobrzański and L. Maccone, Using entanglement against noise in quantum metrology, *Phys. Rev. Lett.* **113**, 250801 (2014).
- [37] S. L. Braunstein and C. M. Caves, *Statistical distance and the geometry of quantum states*, Vol. 72 (1994) pp. 3439–3443.
- [38] J. Liu, X.-X. Jing, W. Zhong, and X.-G. Wang, Quantum Fisher Information for Density Matrices with Arbitrary Ranks, *Commun. Theor. Phys.* **61**, 45 (2014).

SUPPLEMENTARY MATERIAL

Evolution of the purity and entanglement entropy with the environment

Purity of a density matrix ρ is given by $\text{Tr}[\rho^2]$ and can be expressed in terms of the eigenvalues λ_k as $\mathcal{P} = \sum_k \lambda_k^2$. The evolved dephased bare GHZ state has eigenvalues

$$\lambda_0 = (1/2)(1 - (1 - p)^N) \quad (\text{S1})$$

$$\lambda_1 = 1 - \lambda_0 \quad (\text{S2})$$

leading to $P(\rho^N(p)) = \frac{1}{2}(1 + (1 - p)^{2N})$. On the other hand, the transversal state has eigenvalues given by

$$\lambda_k = (1 - p/2)^{N-k}(p/2)^k + (1 - p/2)^k(p/2)^{N-k} \quad (\text{S3})$$

with $0 \leq k \leq N - 1$ (each with a degeneracy of $\binom{N-1}{k}$) leading to a purity $P(\rho_T^N(p)) = \left(p^N(1 - \frac{p}{2})^N + (1 - p + \frac{p^2}{2})^N\right)$. Although both purities decay exponentially with N , the purity of the bare state tends to $1/2$, while the purity of transversally encoded state tends to 2^{1-N} . The entanglement between system and environment can also be quantified via the von Neumann entropy of the system

$$S(\rho) = \text{Tr}(\rho \log_2 \rho) = - \sum_k \lambda_k \log_2 \lambda_k. \quad (\text{S4})$$

For this quantity, closed formula expressions are not any longer possible but one can easily see some interesting properties. For the bare GHZ state the entanglement entropy tends to $S(\rho_N(p)) = 1$ while for the encoded state $S(\rho_N^T(p)) = N - 1$ as $p \rightarrow 1$. Moreover, for any p it follows that $S(\rho_N^T(p)) > S(\rho_N(p))$, that is, at all times of the noisy evolution the encoded and more robust state is surprisingly more entangled with the environment.

Negativity analysis

For both the GHZ state and Linear Cluster, we consider all the 1-vs-rest partitions ($i|jkl$) and 2-vs-2 bipartitions : ($12|34$), ($13|24$), ($14|23$). The transversal 4-GHZ state is optimally protected in both all the 1-vs-rest and 2-vs-2 partitions. The scenario is more complex when instead we study the linear cluster, in fact there always exists at least one 1-vs-rest partition where the protection is optimal. However, the partition depends from the encoding chosen. Nevertheless, encoding providing protection for all the 1-vs-rest partitions exist, but the protection is not optimal.

Robustness of multilevel coherence

Following Ref. [34], we now review the concept of multilevel quantum coherence as a fine-grained quantifier for

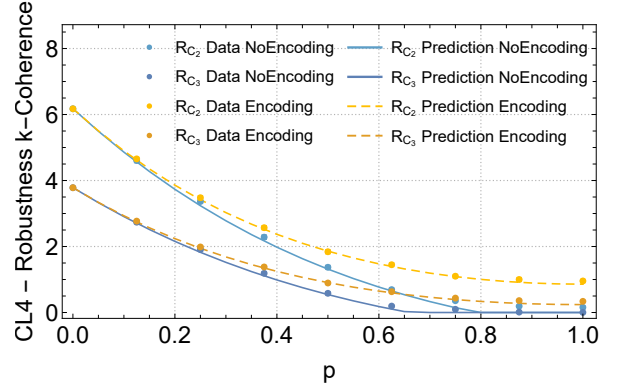


FIG. S1. **Robustness of multilevel coherence.** Shown is the robustness of 3-level (R_{C_2}) and 4-level (R_{C_3}) coherence the bare (blue) and encoded (orange) linear cluster. Similar to the results in the main text, the encoding provides enhanced protection of coherence at all levels and for all values of p . Experimental data is shown as dots with 3σ error bars.

the amount of coherence present in a given quantum state. We consider composite N -qubit systems and measure coherence with respect to the computational basis $\{|0\rangle, |1\rangle\}^{\otimes N}$. In order to capture the structure of coherence in such a system, one first defines the following sets of states

$$\mathcal{C}_k := \text{conv}\{|\psi\rangle\langle\psi| : r_c(|\psi\rangle) \leq k\}, \quad (\text{S5})$$

where conv stands for convex hull and r_c is the coherence rank of $|\psi\rangle$, given by the number of non-zero coefficients in the basis-decomposition of $|\psi\rangle$. \mathcal{C}_1 is the set of fully incoherent states, given by density matrices that are diagonal in the computational basis, while $\mathcal{C}_d \equiv \mathcal{D}(\mathcal{H})$ is the set of all states in the d -dimensional Hilbert space \mathcal{H} . It was shown in Ref. [34] that these sets obey a strict hierarchy and that the amount of k -level coherence can be quantified by the robustness of multilevel coherence

$$R_{\mathcal{C}_k}(\rho) := \inf_{\tau \in \mathcal{D}(\mathcal{H})} \left\{ s \geq 0 : \frac{\rho + s\tau}{1 + s} \in \mathcal{C}_k \right\}. \quad (\text{S6})$$

Here τ is any density matrix. A state has coherence number k , if it can be decomposed into pure states which are superpositions of at most k basis elements, while every decomposition must contain at least one such state. For $k = 1$, this measure simply quantifies the total amount of coherence in the system and it can be computed efficiently for all k , given the density matrix. For $k = 2$ and $k = 3$ instead the results are shown in Fig. S1. Experimentally, we can quantify the multilevel coherence for a given density matrix using the following semi-definite program, see Ref. [34] for details.

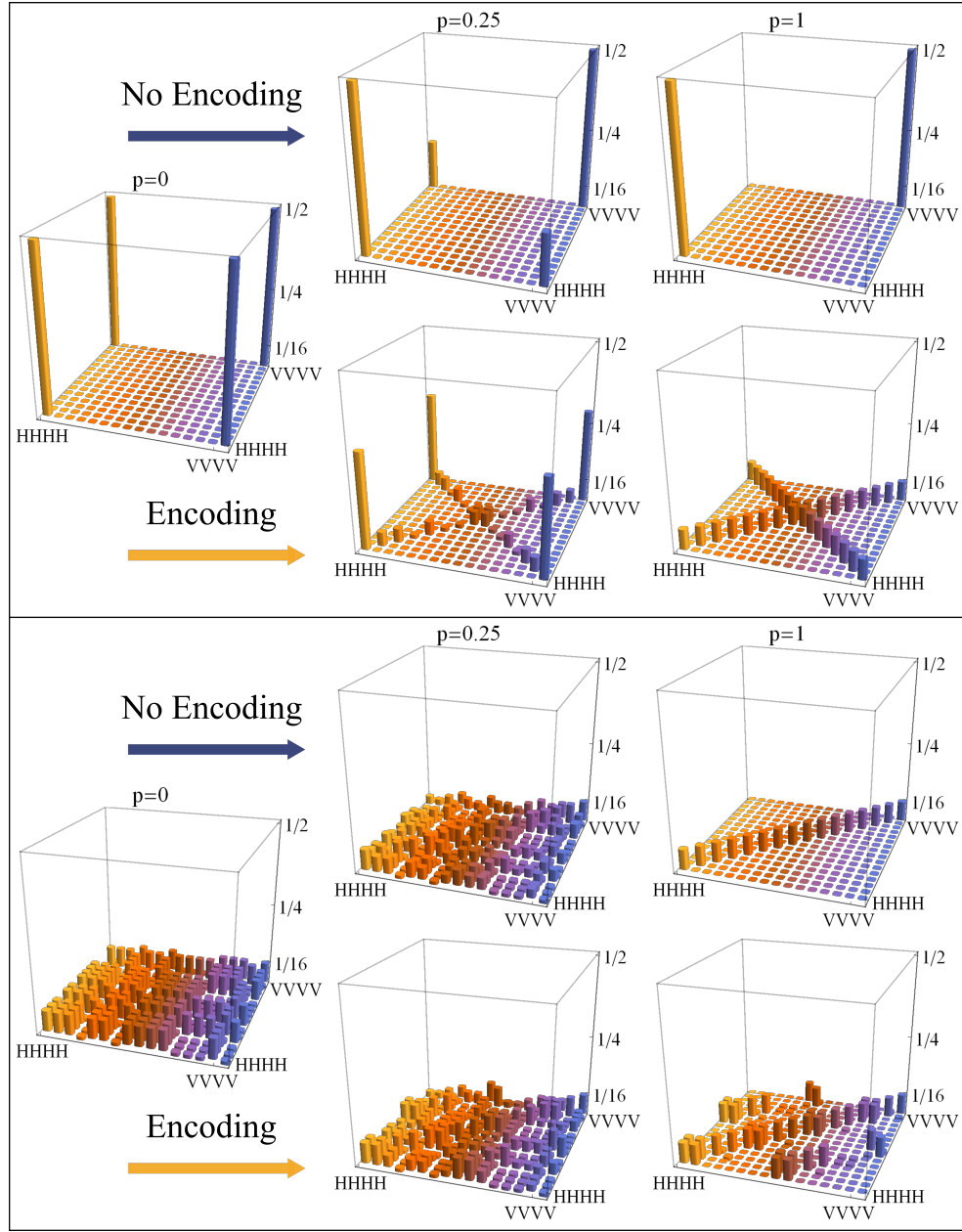


FIG. S2. **Full dephasing density matrices.** Shown are the density matrices of the states for $p = 0, p = 0.25, p = 1$. Top panel, shows the GHZ state without (first row) and with (second row) the encoding. Same, but for the linear cluster, in the bottom panel. The bars on the diagonal show all the 16 populations from $|HHHH\rangle$ to $|VVVV\rangle$ and all the combinations in between whose labels are omitted. Note that, for the linear cluster case, the state naturally produced by our experimental arrangement is the encoded linear cluster rather than the bare state. For this reason the first set of local rotations $H \otimes \mathbb{1} \otimes \mathbb{1} \otimes H$ shown in Fig. 2 should be seen as part of the state preparation rather than an encoding step.